Leukocyte margination in a model microvessel

Jonathan B. Freund
Mechanical Science and Engineering and Aerospace Engineering, University of Illinois at Urbana-Champaign, Urbana, Illinois 61801

(Received 11 March 2006; accepted 9 January 2007; published online 20 February 2007)

The physiological inflammation response depends upon the multibody interactions of blood cells in the microcirculation that bring leukocytes (white blood cells) to the vessel walls. We investigate the fluid mechanics of this using numerical simulations of 29 red blood cells and one leukocyte flowing in a two-dimensional microvessel, with the cells modeled as linearly elastic shell membranes. Despite its obvious simplifications, this model successfully reproduces the increasingly blunted velocity profiles and increased leukocyte margination observed at lower shear rates in actual microvessels. Red cell aggregation is shown to be unnecessary for margination. The relative stiffness of the red cells in our simulations is varied by over a factor of 10, but the margination is found to be much less correlated with this than it is to changes associated with the blunting of the mean velocity profile at lower shear rates. While velocity around the leukocyte when it is near the wall depends upon the red cell properties, it changes little for strongly versus weakly marginating cases. In the more strongly marginating cases, however, a red cell is frequently observed to be leaning on the upstream side of the leukocyte and appears to stabilize it, preventing other red cells from coming between it and the wall. A well-known feature of the microcirculation is a near-wall cell-free layer. In our simulations, it is observed that the leukocyte's most probable position is at the edge of this layer. This wall stand-off distance increases with velocity following a scaling that would be expected for a lubrication mechanism, assuming that there were a nearly constant force pushing the cells toward the wall. The leukocyte's near-wall position is observed to be less stable with increasing mean stand-off distance, but this distance would have potentially greater effect on adhesion since the range of the molecular binding is so short.
[DOI: 10.1063/1.2472479]

I. BACKGROUND

A key part of the physiological process of inflammation is the recruitment and adhesion of leukocytes (white blood cells) to the endothelial lining of the microvasculature. This occurs primarily in the postcapillary venules, which have diameters only several times larger than the cell dimension. Once in contact, leukocytes can interact directly with the endothelium via selectin-ligand bonds. These bonds are weak and few enough that leukocytes may roll along the endothelium at this stage. Later, it may become firmly attached in a second stage if stronger integrin mediated bonds are activated by chemoattractants released by the endothelium.[1] These stop the leukocyte in the flow and eventually it deforms and exits the vessel through the endothelium into the tissue beyond. The chemical mechanism involved are important and well studied;[1] the range of the binding, however, is of the nanometer scale, which is far too short to influence how the leukocyte is brought into contact with the endothelium in the first place. This *margination* process involves hydrodynamics and is arguably the rate-limiting factor in the attachment process.[2] (Following Abbitt and Nash,[2] we emphasize margination as distinct from *adhesion* to the vessel wall.) It turns out that under some conditions a remarkably high percentage of leukocytes can be at the wall in the postcapillary venules. Schmid-Schönbein *et al.*,[3] for example, observed 94% margination in 54 μm diameter postcapillary venules of a rabbit ear. However, the leukocyte concentration can also be biased toward the vessel walls in much larger ($\sim$1 mm) vessels.[4]

Since the rheology of blood is dominated by the highly concentrated red blood cells (erythrocytes), which constitute typically about 40% of the blood's volume, interactions with red cells are expected to drive any radial migration of the leukocytes. Stokes flow on its own cannot be the mechanism, because the well-known time reversibility of Stokes flow would not promote margination of relatively stiff and round leukocytes. Small leukocyte deformations can in theory break their symmetry and lead to cross stream transport, but this would be expected to slowly move the leukocyte toward the vessel center,[5] not marginate it. Data taken *in vivo* suggest that leukocyte-erythrocyte interaction plays a key role in the process.[6]

Several studies have examined the effect of shear rate on leukocyte adhesion, and it is clear that low wall shear rates promote adhesion in glass tubes,[7,8] rectangular glass channels,[9] and actual venules in a rat mesentery.[10] The effect of shear in all these cases is dramatic, with an apparently exponential increase in number of adhered cells at smaller shear rates ($\lesssim$100 s^{-1}). A possible explanation for this shear-rate dependence is the well-known property of red cells to aggregate at low shear rates. Supporting this view, it has been observed that the addition of high molecular weight dextran (typically 500 kDa: Dx500) (Refs. 8, 2, and 11) or fibrinogen[12] to the blood, both of which are known to pro-

mote aggregation, also promotes leukocyte adhesion.

It is less clear whether or not red cell aggregation is important at normal physiological shear rates and aggregation conditions. In fact, red cells in some sedentary mammalian species (e.g., sheep or cow) do not tend to aggregate,[13] so we can anticipate that aggregation cannot be the only factor affecting leukocyte margination and adhesion. In their rat mesentery studies, Pearson and Lipowsky[11] measured aggregation with an optical method and saw only a small increase in their aggregation index at the lowest shear rates they studied. Yet leukocyte adhesion increased fourfold, suggesting that aggregation might not be directly responsible. However, in apparent contradiction to this observation, the addition of low molecular weight dextran (40 kDa: Dx40), which inhibits aggregation, still inhibited adhesion even at the lowest shear rates they measured. A possible explanation for this is that a change in the suspending phase viscosity, which is increased by Dx40, directly alters adhesion.[2] Abbitt and Nash[2] suggest that this would be the case if stress were more important than strain rate, though the mechanism remains unclear. The details of this are difficult to investigate since it is difficult to separate aggregation promotion or inhibition from the changes in the rheological properties of the suspending fluid in actual blood. In the present study of a model system, aggregation is strictly omitted.

If aggregation is not a necessary condition for leukocyte margination, it is possibly due only to the different characters of white and red cells that, under some conditions at least, end up pushing the leukocytes toward the vessel walls. Indeed, experiments in a large-scale model system[3] have suggested that specific erythrocyte-leukocyte interactions can do this. Similarly, Sun *et al.*[14] report a numerical simulation in which they observed red cells, which tend to pile up behind slower moving leukocytes in the capillaries, pushing the leukocyte toward the wall after an expansion. Only a small number of rigid and regularly shaped red cells were simulated in their two-dimensional model, but it was clear that they could have a significant impact on leukocyte margination. Hydrodynamic interactions are also important in the rolling and adhesion stages that occur after margination, which have also been studied with simulations,[15–17] but are not considered in the current effort. Other noteworthy efforts have attempted to simulate deformable red cells, but without direct application to leukocyte transport.[18–20]

The first objective of the present study is to test if aggregation is necessary for leukocyte margination. The simulation model we employ to study this is introduced in Sec. II. It is two-dimensional with cell properties that are idealized in several ways, but we will show that despite these unphysiologic approximations it captures several of the key features of flow and leukocyte transport in the microcirculation and so can be used to investigate flow phenomenology of potential physiological importance. Once validated in this way, the simulation model is particularly useful because it is free from any ambiguity concerning the roles of shear rate, stress and aggregation. We show that aggregation per se is not necessary, and will suggest instead that the relative properties of the leukocytes and erythrocytes alone can cause margination. We examine the mechanisms by which this occurs and the factors governing the time spent by the leukocyte in near contact with the vessel wall. The simulation results are presented and discussed in Secs. III and IV and summarized in Sec. V.

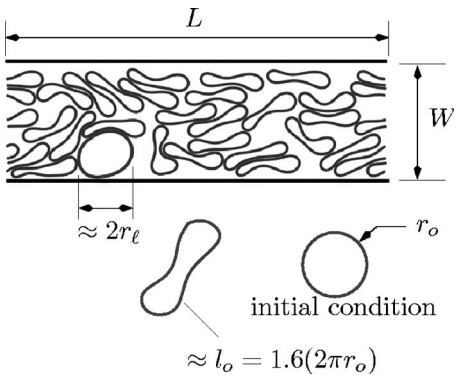

FIG. 1. System schematic.

II. THE MODEL SYSTEM

A. Physical details

Our model system is shown in Fig. 1. It is a two-dimensional streamwise-periodic channel of length L and width W. For all cases presented, there are 29 two-dimensional red cells each with cross-sectional area πr_o^2, and one leukocyte with cross-sectional area πr_ℓ^2. We expect quantitative differences between this two-dimensional model and actual three-dimensional blood flow, but we will show that it gives phenomenologically correct leukocyte margination and near-wall cell-free layers. The average hematocrit is $H_c = 0.45$, which is higher than many observations in the microcirculation[21,22] but leukocyte behavior has been shown to be insensitive to H_c.[2] We will also briefly present results at $H_c = 0.33$ and 0.22 to confirm insensitivity of the basic phenomenology to H_c. Actual blood cells have an internal viscosity that is several times larger than the surrounding plasma, but to simplify the formulation and speed its numerical solution we assume that they have the same Newtonian viscosity μ inside and out. This does not stop the model from reproducing key features of the microcirculation, and we shall see that our results in general are relatively insensitive to the red cell properties. Flow in the microcirculation is low Reynolds number and therefore assumed to be Stokesian and, of course, incompressible.

The cells are modeled with a linear elastic membrane with tension

$$\tau = T\left(\frac{ds}{ds_o} - 1\right), \tag{1}$$

where T is the tension modulus, $s(s_o)$ is the arc length of the membrane, and s_o is the referential arc-length coordinate measured around the l_o perimeter of a hypothetical tension-free membrane. For $l_o > 2\pi r_o$, the membranes would buckle were it not for their resistance to bending. The bending moment in our model is

$$b = M(C - C_o), \tag{2}$$

where M is the bending modulus and $C = C(s_o)$ is the local membrane curvature. The reference curvature C_o is assumed to be constant and does not affect the dynamics of our system. For the leukocyte, moduli T and M for the red cells are replaced by T_ℓ and M_ℓ. The membranes are assumed to have no mass, and therefore move at the local fluid velocity. Their influence on the flow is thus only through the surface stress they apply on the fluid.

Overall, we have defined 10 geometrical and material parameters in our system: M, T, r_o, M_ℓ, T_ℓ, r_ℓ, l_o, μ, W, L, and H_c. To drive the flow, we assume that in the absence of the cells and channel walls there would be a uniform velocity of u^∞. This sets up a streamwise pressure gradient, which is related to the wall strain rate,

$$\sigma_w \equiv \left.\frac{\partial u}{\partial y}\right|_{\text{wall}}, \tag{3}$$

by the viscosity. Using r_o, T, and (for now) u^∞ to nondimensionalize, all the physical parameters can be formed into 9 nondimensional groups, most of which are held constant throughout this study.

The nondimensional geometric parameters are

$$\frac{W}{r_o} = 7.8 \quad \frac{L}{r_o} = 27 \quad \frac{r_\ell}{r_o} = 1.75 \quad \frac{l_o}{r_o} = 1.6 \times 2\pi. \tag{4}$$

This red-cell reference length l_o was selected to give them a characteristic biconcave shape at equilibrium. The leukocyte size and material properties are such that it remains nearly circular. Appropriate values for geometric parameters can be easily estimated.[23,24] Because the leukocyte's geometry is essentially fixed, no dependence of the results on M_ℓ and T_ℓ is expected. This was confirmed directly and is briefly revisited in Sec. IV B. In most cases, $T_\ell/T > 6$ and $r_o^2 T_\ell/M_\ell > 30$, but the leukocytes also had r_ℓ such that $2\pi r_\ell > l_o$, so their membranes were always in relatively high tension. Actual red cells have nearly incompressible membranes, but it is convenient to model them with tension modulus T simply being much more restrictive than bending modulus M. In all cases, we set $r_o^2 T/M = 50$. Switching to $r_o^2 T/M = 100$ causes a less than 1% change in the mean velocity profile for case **a1** in Table I, which has the relatively most flexible cells and is therefore presumably most sensitive to the stretching. Precise agreement is neither expected nor sought, but taking $M = 1.8$ dyn cm,[5] $r_o = 1.75$ μm, and $\mu = 0.0013$ kg/(m s) (Ref. 25) as reasonable dimensional values for blood cells and plasma, the velocities we discuss later in the paper are similar to observations for flow in vessels with similar diameter.[25] For example, for case **a1** the peak velocity corresponds to $U \approx 0.025$ cm/s for microvessels with width 14 μm.

The main parameters we varied in the different cases we considered were u^∞ and T (with T/M fixed). To discuss the relative shear, advection and red cell flexibility of the cases simulated, we define advective, wall-shear, and relaxation time scales:

TABLE I. Cases simulated. The *-marked cases indicate a series with constant cell properties.

Case	$\frac{\mu u^\infty}{T}$	$\frac{\tau_{\text{rlx}}}{\tau_{\text{sh}}} = \frac{\mu r_o \sigma_w}{T}$	$\frac{\tau_{\text{rlx}}}{\tau_{\text{adv}}} = \frac{\mu \bar{u}_m}{T}$	$\frac{\tau_{\text{adv}}}{\tau_{\text{sh}}} = \frac{r_o \sigma_w}{\bar{u}_m}$	N	N_a
a1*	0.80	0.120	0.109	1.10	32	128
a2		0.120	0.106	1.13		
a3		0.115	0.100	1.15		
a4		0.114	0.094	1.21		
a5		0.122	0.084	1.44		
b*	0.60	0.090	0.077	1.16	32	128
c*	0.40	0.060	0.039	1.45	32	128
d1	0.20	0.028	0.020	1.40	20	80
d2*		0.0281	0.017	1.64		
d3		0.0245	0.014	1.73		
e*	0.067	0.0073	0.0036	2.02	20	80
f1	0.05	0.0055	0.0040	1.36	16	64
f2		0.0057	0.0037	1.54	16	64
f3		0.0053	0.0032	1.64	20	80

$$\tau_{\text{adv}} \equiv \frac{r_o}{\bar{u}_m} \quad \tau_{\text{sh}} \equiv \frac{1}{\sigma_w} \quad \text{and} \quad \tau_{\text{rlx}} \equiv \frac{\mu r_o}{T}. \tag{5}$$

The imposed u^∞ is only indirectly related to the actual centerline velocity $\bar{u}_m$ and this relationship changes with T, which can be thought of as altering the overall constitutive properties of the suspension. A nonlinear relation is expected because of the well-known non-Newtonian character of suspensions like blood.

Table I summarizes the cases simulated, which are organized as follows. The case letter (**a**-**f**) indicates significantly different cell relaxation time scales relative to flow time scales, with **a** corresponding to the slowest relative relaxation. The **a**, **d**, and **f** cases are broken into subcases, which are designated by numbers that increase monotonically with increasing profile bluntness, as measured by the relative advection and wall-shear time scales. More blunt profiles can be considered in some sense less Newtonian, because they are further from the parabolic profile expected for Newtonian fluids. In practice, blunter flows were obtained by fixing $\mu u^\infty/T$ but decreasing u^∞.

The boundary integral formulation we employ in the numerical discretization becomes expensive if cells come close together because of the number of quadrature points required on the membranes to accurately evaluate nearby velocities. For this reason, we added a short-range repulsion between all of the membranes and walls in the calculation. An electrostatic repulsion is known to exist between actual red blood cells,[26] but it appears to act over a very short ~20 nm range. Accurately resolving hydrodynamics interactions at this range would require a prohibitive number of quadrature points, whose requisite density scales approximately as δ. For our model, the force on point $\mathbf{x}$ on one membrane due to point $\mathbf{x}'$ on another membrane is

$$\mathbf{f}(\mathbf{x}) = \begin{cases} S_f \dfrac{e^{\delta - r} - 1}{e^{\delta} - 1} \dfrac{\mathbf{x} - \mathbf{x}'}{r} & \text{for } r \le \delta, \\ 0 & \text{for } r > \delta, \end{cases} \tag{6}$$

where $r = |\mathbf{x} - \mathbf{x}'|$ and δ and S_f are the length scale and magnitude of the force. For all cases, $\delta = 0.2 r_o$ and $S_f / r_o T > 3.33$. This force is integrated over the membrane and modifies the traction of the membranes on the fluid $\Delta\boldsymbol{\sigma}$. The selected S_f was strong enough to prevent cells from coming much closer than δ. Removing the surface charge of actual cells has been shown to accelerate axial accumulation of red cells and the thickness of the marginal nearly cell-free layer,[27] so imposing our potential with $\delta = 0.2 r_o$ is expected to affect the dynamics somewhat. However, simulations with $\delta = 0.1 r_o$ show the same margination behavior (Sec. III C), and we shall see in general that our physiologically large repulsion range does not stop the simulations from reproducing the key qualitative features of interest in the microcirculation.

B. Numerical flow solution

1. Boundary integral discretization

The boundary integral expression for the velocity due to surface tractions in a uniform viscosity Stokes flow is well known (e.g., Pozrikidis[28]):

$$u_i(\mathbf{x}) = u_i^{\infty} + \frac{1}{4\pi\mu} \int_{\Omega} S_{ij}(\mathbf{y} - \mathbf{x}) \Delta\sigma_j(\mathbf{y}) ds(\mathbf{y}). \tag{7}$$

Here $u_i(\mathbf{x})$ is the velocity vector at point $\mathbf{x}$, $u_i^{\infty} = (u^{\infty}, 0, 0)$ is the uniform flow that would exist in the absence of surface(s) Ω, and μ is the Newtonian viscosity. The integral is a convolution of the Green's function of the Stokes equation (the so-called *Stokeslet*) S_{ij} with the traction $\Delta\sigma_j$ exerted by the membranes on the fluid.

In two dimensions, it is convenient to parameterize each membrane shape Ω by a reference arc length s_o. The membrane can stretch (though not much for our parameters) into a curve of arc length $s(s_o)$ with its position defined simply as $\mathbf{x}(s_o)$. We discretize this continuous shape by N evenly spaced points in s_o for each cell: $\mathbf{x}^m = \mathbf{x}(s_o^m)$ for $m = 1, \ldots, N$. To compute derivatives and integrals on the membranes, we assume that these N points are interpolated by harmonic functions and employ Fourier methods. This has three main advantages: (1) optimal computational efficiency for a given accuracy, (2) consistent high-resolution quadratures, and perhaps most importantly (3) a means of countering aliasing errors without application of dissipative filters. The first advantage is clear. Fourier spectral methods are well known to be optimally accurate for representing smooth periodic functions, such as the membrane shape, on evenly spaced points. Our approach thus reduces the number of collocation points for a given accuracy, which affords savings both directly in the computational work per time step and via the time-step stability constraint for explicit time integration.

For the flow considered, we found that the shapes taken by the cells were significantly less challenging to resolve than the integrand of (7), which we therefore evaluated with $N_a > N$ quadrature points. Fourier spectral interpolation was used at the intermediate points to compute $\mathbf{x}$ and $\Delta\boldsymbol{\sigma}$ values that are exactly consistent with the underlying harmonic interpolants. The resulting quadrature used is a simple sum around each cell,

$$u_i^m = u_i^{\infty} + \frac{1}{4\pi\mu} \sum_{n=1}^{N_a} S_{ij}(\mathbf{x}^{nm}) \Delta\sigma_j^n \left. \frac{ds}{ds_o} \right|^n \Delta s_o \quad \text{for } m = 1, \ldots, N, \tag{8}$$

where superscripts n and m denote the discrete points on the membrane and we define $\mathbf{x}^{nm} \equiv \mathbf{x}^n - \mathbf{x}^m$. The Green's function S_{ij} has an integrable singular behavior at $n = m$, which we treat analytically in the usual way,

$$\begin{aligned} u_i^m = u_i^{\infty} + \frac{1}{4\pi\mu} \sum_{n=1}^{N_a} \Bigg[& S_{ij}(\mathbf{x}^{nm}) \Delta\sigma_j^n \left. \frac{ds}{ds_o} \right|^n \\ & - \widetilde{S}_{ij}(\mathbf{x}^{nm}) \Delta\sigma_j^m \left. \frac{ds}{ds_o} \right|^m \Bigg] \Delta s_o \\ & + \Delta\sigma_j^m \left. \frac{ds}{ds_o} \right|^m \int_{\Omega} \widetilde{S}_{ij}(\mathbf{x}^{nm}) ds_o, \end{aligned} \tag{9}$$

where $\widetilde{S}$ has the same singularity as S. This preserves the spectral properties of the quadrature. The integral of $\widetilde{S}$ in the final term is evaluated accurately once and reused. The spacing Δs_o is constant around any periodic cell membrane, but in general can vary from cell-to-cell and on the vessel walls.

It was observed that nonlinearity in the membrane dynamics equations and the integrand of (7) lead to a slow growth of deformation energy via aliasing. By this process, unresolvable high wave number energy, which is created by nonlinearity, is artificially aliased by the discretization into resolved wave numbers. If this aliased energy is not explicitly removed, it provides a mechanism for instability, which by its nature is typically observed in the highest resolved wave numbers and over relatively long simulation times. Dealiasing[29] algorithms attempt to remove this unresolvable energy before it is aliased, leaving resolved deformations unaffected. An alternative stabilization procedure that can be used is smoothing of the membrane shapes. Such filters remove high wave number energy outright, but unless they are Fourier spectral filters they also affect the dynamics of all deformation scales. The highest wave number deformations in particular are rendered inaccurate by any such filtering, yet they must be computed and still typically restrict the numerical time step via the standard constraint for explicit time integration. Dealiasing is probably the most important component of our algorithm and has enabled us to compute long enough time series to converge leukocyte transport statistics.

In our model, the membranes are assumed to have no mass, so their traction on the fluid depends only upon the membrane configuration. The membrane position thus evolves simply according to $\partial_t \mathbf{x} = \mathbf{u}(\mathbf{x})$. For a shell membrane $\mathbf{x}(s)$, the traction is

$$\Delta\boldsymbol{\sigma} = \frac{\partial \mathbf{t}\tau}{\partial s} + \frac{\partial}{\partial s}\left(\frac{\partial b}{\partial s}\mathbf{n}\right), \tag{10}$$

where $\mathbf{t}$ is a unit tangent, $\mathbf{n}$ is a unit normal, and τ and b are defined in (1) and (2), respectively. Each derivative is computed by discrete Fourier transforming from s_o to κ coordinates, multiplying by $i\kappa$ and inverse transforming. Though (10) is relatively simple per se, evaluating it entails several nonlinear operations, which gives $\Delta\boldsymbol{\sigma}(s_o)$ around any particular cell a significantly broader spectrum than $\mathbf{x}(s_o)$ and leads to aliasing. To minimize this, we compute $\Delta\boldsymbol{\sigma}(s_o)$ on $N_a > N$ points and filter down to N points as necessary after every potentially aliasing operation. This procedure is exact for products but only approximate for the quotients and square-roots computed in forming (10), though in practice it is nearly perfect anyway since $N_a = 4N$ for all our cases. The specific N_a and N for the various cases are listed in Table I. A similar procedure was used to dealias the integrands.

Though we will later restrict this to form the walls of our channel, our formulation starts with the domain being periodic in all directions. Following Hashimoto,[30] an appropriately periodic form of the Stokes Green's function is

$$S_{ij}(\mathbf{x}) = \underbrace{E_1\left(\frac{\pi|\mathbf{x}|^2}{\alpha}\right)\frac{\delta_{ij}}{2} + e^{-\frac{\pi|\mathbf{x}|^2}{\alpha}}\left(\frac{x_i x_j}{|\mathbf{x}|^2} - \delta_{ij}\right)}_{S^r_{ij}} + \frac{1}{\pi A}\sum_{\mathbf{k}\neq 0} e^{-i2\pi\boldsymbol{\kappa}\cdot\mathbf{x}} \underbrace{\frac{\kappa^2\delta_{ij} - \kappa_i\kappa_j}{\kappa^4}(1 + \pi\alpha\kappa^2)e^{-\pi\alpha\kappa^2}}_{G_{ij}(\boldsymbol{\kappa})}, \tag{11}$$

where A is the area of the periodically repeated $L\times L$ domain, $\boldsymbol{\kappa} = \mathbf{k}/L$ is the wave number vector with $\kappa^2 = \boldsymbol{\kappa}\cdot\boldsymbol{\kappa}$, E_1 is

$$E_1 = \int_1^\infty \frac{e^{-x\xi}}{\xi} d\xi, \tag{12}$$

and α is a free parameter that can be adjusted to optimize the efficiency of the complete numerical scheme. In writing (11), we have assumed that α is small enough that S^r becomes negligible at least by $|\mathbf{x}| = L$. Only the E_1 term of (11) is singular, so combining (11) with (8) yields

$$\begin{aligned} u_i^m = \; & u_i^\infty - \frac{1}{4\pi\mu}\sum_{n=1}^{N_a}\left[S^r_{ij}(\mathbf{x}^{nm})\Delta\sigma_j^n\frac{ds}{ds_o}\bigg|^n - \tilde{S}^r_{ij}(\mathbf{x}^{nm})\Delta\sigma_j^m\frac{ds}{ds_o}\bigg|^m\right]\Delta s_o^n \\ & - \Delta\sigma_j^m\frac{ds}{ds_o}\bigg|^m\int_\Omega \tilde{S}^r_{ij}(\mathbf{x}^{nm})ds_o \\ & - \frac{1}{4\pi\mu}\frac{1}{\pi A}\sum_{\mathbf{k}\neq 0} G_{ij}(\boldsymbol{\kappa})e^{i2\pi\boldsymbol{\kappa}\cdot\mathbf{x}^m}\underbrace{\sum_{n=1}^{N_a}\Delta\sigma_j^m e^{-i2\pi\boldsymbol{\kappa}\cdot\mathbf{x}^n}}_{F_j(\boldsymbol{\kappa})}. \end{aligned} \tag{13}$$

L'Hopital's rule is employed as necessary for the $n=m$ points.

The computational expense of this formulation for evaluating u_i depends not just on the number of points N_a, but also upon their density in physical space and the necessary number of wave vectors needed to sufficiently converge the G sum. The value of α sets both the range of interactions that need to be considered in the first sum and the number of Fourier modes that must be retained in the second. All other parameters being fixed, an α can be found such that the total expense should scale as $O(N^{3/2})$.[31] However, if α is small enough, the terms involving S^r decay rapidly enough to make negligible contribution for $|\mathbf{x}^n - \mathbf{x}^m| > r_c$. They can thus be accurately evaluated accounting only for short-range interactions. To compute these in practice, a list of near-neighbors is constructed with an $O(N)$ algorithm and then used when evaluating S^r for any u_i^m. Since for small r_c each point m has a small number of neighbors n, this whole portion of the algorithm will have an operation count that scales as $O(N)$. For the results presented, we used $\alpha = 0.042r_o^2$ and $r_c = 0.5r_o$.

The evaluation of the second part of the sum in (13) can be accelerated by formulating it on a regular mesh and using fast Fourier transforms (FFTs), which yields an $O(N\log N)$ algorithm. This involves distributing the $\Delta\boldsymbol{\sigma}$ to the mesh, applying a FFT to compute $F_j(\boldsymbol{\kappa})$ in (13), multiplying to form F_jG_{ij}, inverse transforming, and interpolating back to the $\mathbf{x}^m$ points. Errors incurred in the interpolation phases can be reduced by modifying G_{ij} in a way that partially negates them. This basic approach has been used for simulating n-body systems of various kinds and is known as the particle-particle/particle-mesh (P^3M) method[32] or the closely related particle mesh Ewald (PME) method.[33] It has also been applied to several Stokesian flow systems.[34,35] Our formulation is most similar to that of Metsi,[35] with the key difference that we used B-spline interpolants as proposed by Hockney and Eastwood.[32] These are also clearly explained within the PME framework for Stokes flow by Saintillan *et al.*[34] The simulations in this paper all used second-order B-splines with square mesh spacing $\Delta = 0.15r_o$.

2. Wall boundaries

To include walls, images of Green's functions can be included (e.g., Staben *et al.*[36]), but this yields intractable summation series for all but the simplest geometries. Imposition of no-slip boundaries is significantly easier if the boundary positions are not forced to be exactly fixed and instead are allowed to flex an arbitrarily small amount. Walls, for example, could be constructed as stiff membranes, but this would impose a significant time-step restriction for explicit time integration. Instead, we construct walls made of Δs_w elements that are not dynamically coupled to each other by any equation such as (10). Instead, they are only fixed to their desired location $\mathbf{x}^w$ by a virtual spring, so that

$$\Delta\boldsymbol{\sigma}_w = -k_w(\mathbf{x} - \mathbf{x}^w). \tag{14}$$

With this $\Delta\boldsymbol{\sigma}_w$, the velocity is evaluated as for all the other surface points in the computation, which simplifies the algorithm. The value of the spring constant k_w can be large since it is only restricted by the ordinary differential equation stability limit of the time integrator. The walls we made with

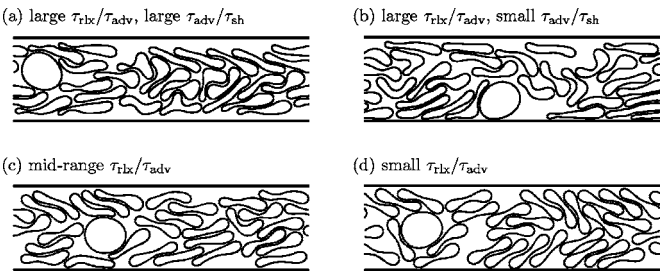

FIG. 2. Sample visualizations of cases from Table I: (a) **a1**, (b) **a5**, (c) **d2**, and (d) **f3**. Plotted are the discrete quadrature points, interpolated from the control points, which define the cells as discussed in Sec. II B. Flow is from left to right.

this method removed the implied periodicity of (13). Results were verified to be insensitive to k_w by doubling it and halving the time step. In spirit, the formulation is similar to a penalty method of the type used commonly in finite-element formulations.

3. Cell area constraint

Though the integral formulation (7) formally preserves the area of the two-dimensional cells, its discrete form (13) does this only approximately. Time step to time step these errors are negligible, but their accumulation over tens of thousands of time steps can invalidate the solution. To counter this, we constrained the area of every cell,

$$A = \frac{1}{2}\int_{\Omega_c} \mathbf{x}\cdot\mathbf{n}\,ds, \tag{15}$$

by seeking perturbations $\mathbf{z}$ that minimize

$$I = \lambda\left[\int_{\Omega_c}\frac{1}{2}(\mathbf{x}+\mathbf{z})\cdot\mathbf{n}\,ds - A_o\right] + \int_{\Omega_c}\mathbf{z}\cdot\mathbf{z}\,ds, \tag{16}$$

where A_o is the initial area of the particular cell and λ is a Lagrange multiplier. The variation of I,

$$\delta I = \delta\lambda\left[\int_{\Omega_c}\frac{\mathbf{z}\cdot\mathbf{n}}{2}ds + (A-A_o)\right] + \int_{\Omega_c}\delta\mathbf{z}\cdot\left(2\mathbf{z}+\frac{\lambda}{2}\mathbf{n}\right)ds, \tag{17}$$

is zero for the $\mathbf{z}$ we seek. For arbitrary $\delta\mathbf{z}$, the second term gives $\mathbf{z}=-\lambda\mathbf{n}/4$, and with this and for arbitrary $\delta\lambda$, the first term gives $\lambda=8(A-A_o)/P$, where P is the perimeter of the cell before the correction. Since $\mathbf{z}\propto\mathbf{n}$, this correction does not change $\mathbf{n}$, which is consistent with neglecting the variation of $\mathbf{n}$ in (17). This constraint was applied every time step, making corrections to the area of typically less than 1 part in 10^5.

III. RESULTS

A. Visualizations

Figure 2 shows visualizations of the cell positions for four of the cases listed in Table I. These were selected to illustrate (a) a less blunt mean flow case (large τ_{adv}/τ_{sh}) with relatively flexible red cells in which the leukocyte has a low probability of being on the wall, (b) more blunt mean flow case (small τ_{adv}/τ_{sh}) with flexible red cells in which the leukocyte is almost always on the wall, (c) a case with medium stiffness cells, and finally (d) a case with unphysiologically stiff cells. The need for greater resolution in the discretization of the flexible cell cases [Figs. 2(a) and 2(b)] is clear. These are closer to the large deformations seen at physiologic conditions. It is also clear that in these cases the imposed short-range repulsion between membranes (6) is also active at times between different parts of a single cell's membrane. The stiffer cells shown in Figs. 2(c) show increasingly the biconcave equilibrium shape expected for the red blood cells. These less physiologic stiff-cell cases were simulated for contrast to assess the importance of cell flexibility for margination.

B. Mean velocity profiles

Velocity fields can be calculated using the same formulation presented in Sec. II B. We see in Fig. 3 that the velocity profile is blunted, as expected for blood flow (e.g., Popel

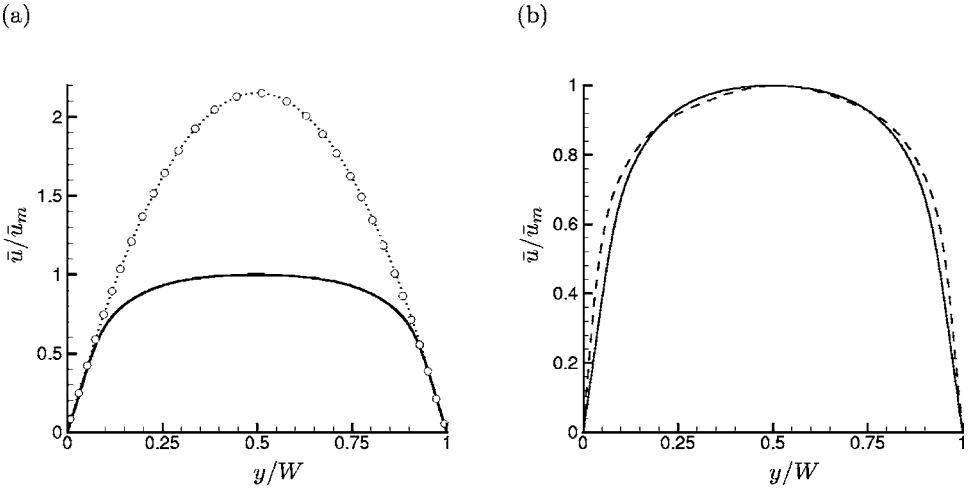

FIG. 3. (a) Mean velocity profile for case **a1**, —; the ○ show the velocity profile calculated in the absence of cells, just using the forces from (14) with parabolic fit ⋯. (b) Case **a1**, — is contrasted with the slower flowing case **d2**- - -.

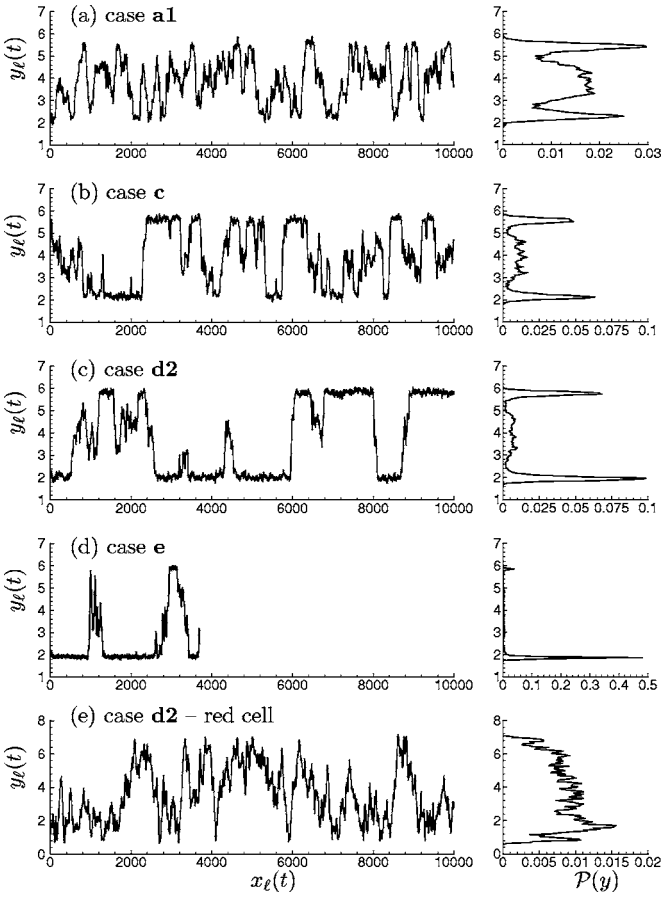

FIG. 4. (a-d) Leukocyte centroid trajectories and probability distributions across the model microvessel for the cases as labeled; (e) shows the same for case **d2** as in (c) but for a red cell. In most cases only a part of the simulation time is shown.

and Johnson[37]), having high strain rate near the walls and a relatively flat profile toward the center. Also shown is the mean velocity profile computed using the (14) forces, but omitting the cells. To plotting accuracy, this profile is perfectly fitted by a parabola, as it should be for a Poiseuille flow. The two velocity profiles match up near the wall indicating that the effective viscosity in this region is simply μ, corresponding to a near absence of cells here. This is an aspect of the well-known Fåhræus-Lindqvist effect.[37] The highest shear rate is even more confined to the wall for case **d2**, which was visualized in Fig. 2(c) and had the same T and M. Its velocity profile is plotted in Fig. 3(b). It is well known that blood flow velocities profiles become more blunted in this manner at higher shear rates (e.g., Long[38]).

C. Leukocyte trajectories

The primary concern of this paper is the trajectories of the leukocytes, which are shown in Fig. 4 for several cases. We are particularly interested in what fraction of the time the leukocyte spends near the vessel wall, which can be assessed by the its probability distribution across the channel. It is clear that the simulations have run long enough for there to be hundreds of flowthroughs of the $L=27r_o$ box, even for the slowest flow rate cases. This is long enough to either converge statistics on leukocyte position in cases when it spends

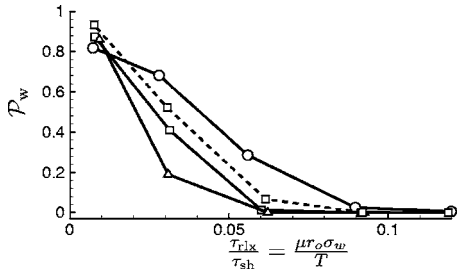

FIG. 5. Probability of leukocyte being within $0.4r_o$ of either wall for the constant cell properties *-marked cases in Table I ○ and for corresponding cases with mean hematocrit 0.33□ and 0.2△. The - - - curve is for cases with $\delta=0.1$ (see text).

considerable time away from the wall or else firmly establish its long-term engagement with the wall. In all cases, the leukocyte traverses the entire channel at least twice, so we assume that it has lost any dependence upon its initial condition.

For fixed cell properties (the *-cases in Table I), different flow speeds give rise to very different leukocyte behavior. At the fastest flow rate of these (case **a5**), the leukocyte's most probable single location is closest to the wall, but it is overall more likely to be away from the wall. The overall on-wall probability increases significantly as the flow rate decreases, as seen in Figs. 4(b)–4(d). In the slowest flowing case shown, the leukocyte spends nearly all its time on the wall and returns to the wall quickly when it occasionally leaves it. The corresponding probability distribution has sharp peaks adjacent to the walls. For contrast, a red cell trajectory for case **d2** is shown in Fig. 4(e). Its probability distribution is relatively flat, and the trajectory is very different than for the leukocyte in the same flow shown in Fig. 4(c).

Experiments with blood have shown rapidly increasing adhesion both *in vivo*[10,11] and *in vitro*[9,39] with decreasing shear rate. Abbitt and Nash's[2] separate measurements of margination and adhesion point to margination as a key, potentially limiting factor in the adhesion process. We do not include adhesion in our model, but we do see a rapid rise in leukocyte margination at lower shear rates. Here, we define a cell as marginated if its closest point is within $0.4r_o$ of a vessel wall. Recalling that the membranes repel at $0.2r_o$ as discussed in Sec. II A, this is only $0.2r_o$ beyond where the leukocyte can be expected to approach. By this measure, the leukocyte in Fig. 2(b) is marginated, for example, but none of the cells near the top wall would qualify were they leukocytes. Using other measures such as different values for this critical distance or criteria based on the centroid probability distributions shown in Fig. 4 does not fundamentally change the following results. Figure 5 shows the probability $\mathcal{P}_w$ that at any given time the leukocyte satisfies this $d<0.4r_o$ margination criterion for the cases with cells with fixed cell material properties. The rapid increase in margination at low flow rates is as observed for adhesion in the experiments. The same behavior is shown for the corresponding lower hematocric ($H_c=0.33$ and $H_c=0.22$) cases, shown in the same plot. In the same figure, we also see that $H_c=0.33$ cases

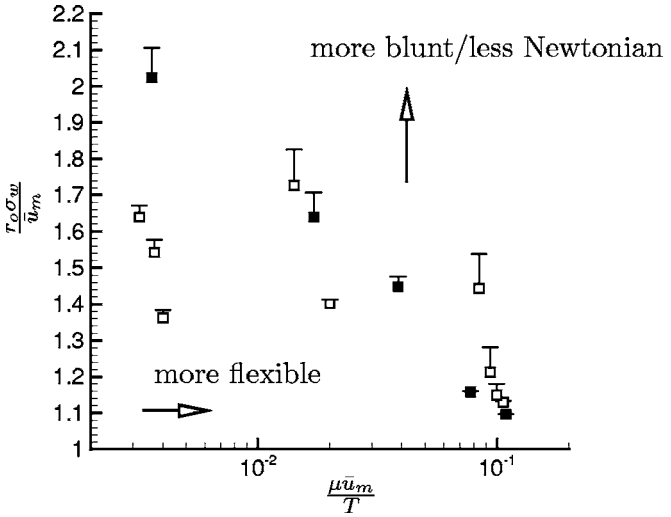

FIG. 6. Marginated probability $\mathcal{P}_w$ of $d<0.4$ for all cases. For each point the bar length is $\mathcal{P}_w/10$ as measured on the vertical axis. The solid ■ correspond to the cases shown in Fig. 5.

with repulsion length scale $\delta=0.1r_o$ in (6) have only slightly higher $\mathcal{P}_w$ than the $\delta=0.2r_o$ cases.

Figure 6 shows $\mathcal{P}_w$ for all the cases listed in Table I. The vertical axis in this figure ($\tau_{adv}/\tau_{sh}=r_o\sigma_w/\bar{u}_m$) is also a measure of deviation from Newtonian behavior, which would give $r\sigma_w/\bar{u}_m=4r_o/W=0.51$. For the relatively firmer cells (smaller $\tau_{rlx}/\tau_{adv}=\mu\bar{u}_m/T$) margination becomes significant at larger τ_{adv}/τ_{sh}, but this change is small compared to the factor of 10 variation in the relative red cell stiffness $\tau_{rlx}/\tau_{adv}=\mu\bar{u}_m/T$. The significance of $r\sigma_w/u_m$ in predicting margination is investigated from a mechanistic perspective involving the near-wall cell dynamics in Sec. IV B.

IV. DISCUSSION

A. Marginated leukocyte environment

We next examine the flow around the leukocyte when it is near the wall, comparing results for cases for which the leukocyte is nearly always near the wall to those for which it has lower probability of being near the wall. Figure 7 shows

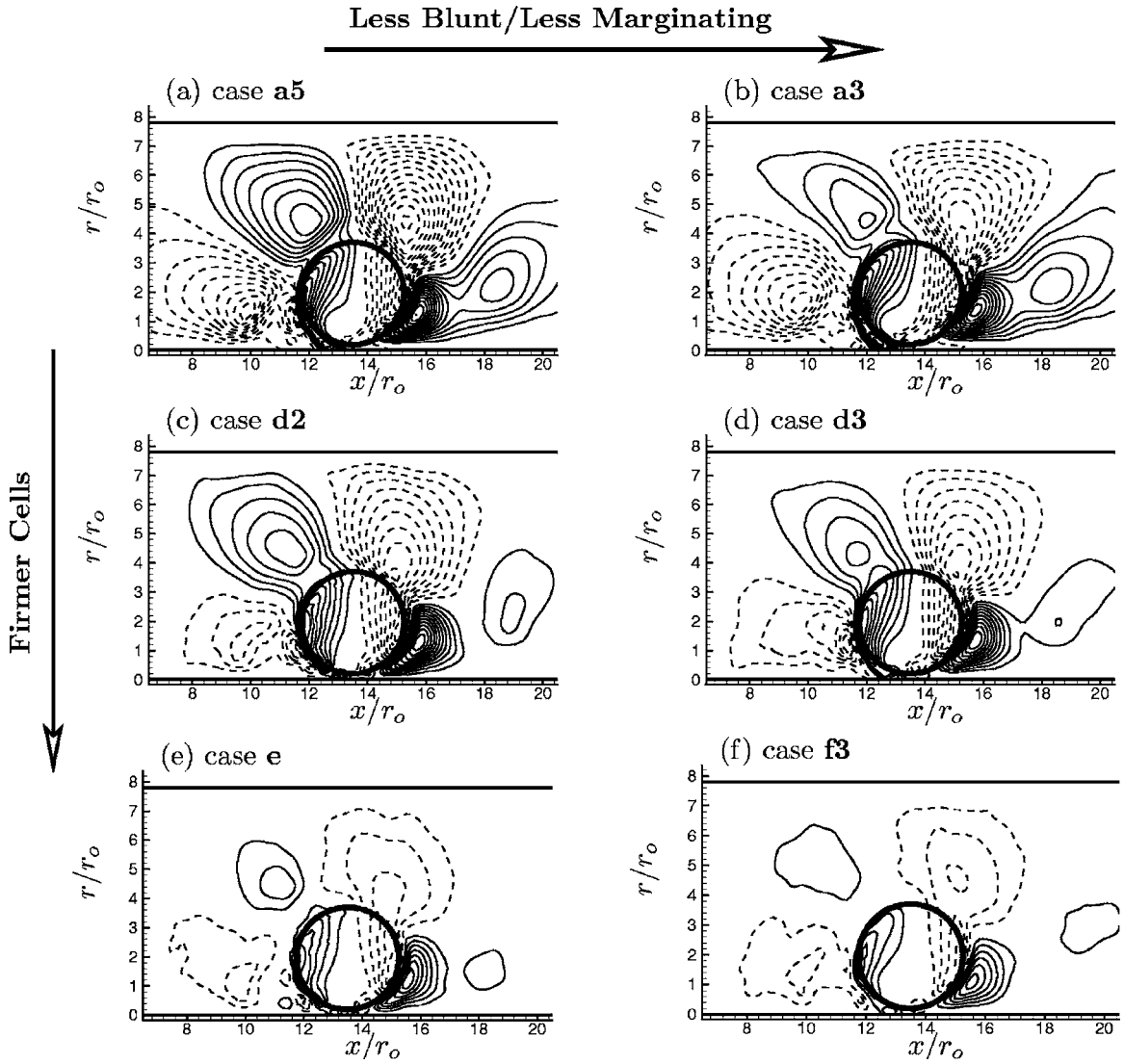

FIG. 7. Contours of mean y-direction velocity $\bar{v}$ averaged on the condition that $d<0.4r_o$ for cases (a) **a5**, (b) **a3**, (c) **d3**, (d) **d2**, (e) **e**, and (f) **f3**. All plots show $\bar{v}/\bar{u}_m$ contours at intervals of 0.001. Negative contours are dashed and the $\bar{v}=0$ contour is not shown.

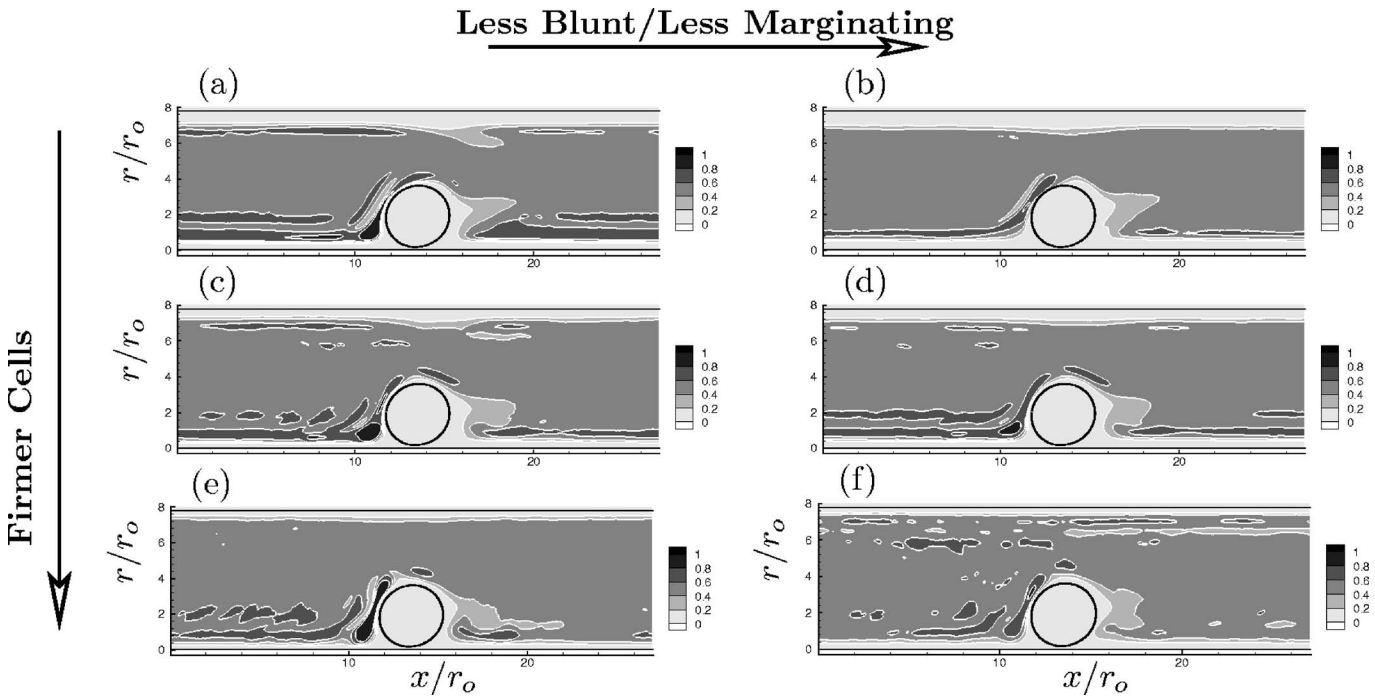

FIG. 8. Local red cell volume density averaged when $d<0.4r_o$ for cases (a) **a3**, (b) **a5**, (c) **d2**, (d) **d3**, (e) **e**, and (f) **f3**. The circle shows the approximate location and shape of the leukocyte, though it does move and deform slightly in the course of the simulation.

the wall normal component of the velocity averaged on the condition that the leukocyte is marginated according to a $d \leq 0.4r_o$ criterion. Comparing the different rows in the figure, it is clear that the red cell stiffness strongly affects the flow around the leukocyte. However, the velocity fields are not obviously different between marginated (plots in the left column) and less-marginated (right column) cases. There is only a slightly larger vertical velocity around the cell for the more marginated cases.

The velocity field differences and the rheological difference they imply are due to cell-scale dynamics. Experiments[3] and simulations[14,17] with few cells suggest that red cell interactions with the leukocyte play an explicit role in margination. The cellular interactions in our model system are more complex, so we have not been able to deduce any single clear multibody mechanisms that pushes the leukocyte toward the wall, but it no doubt involves red cell interactions with the leukocyte. It is not surprising then that we see more significant differences between strongly and weakly marginating cases when we consider the red cells in the neighborhood of the leukocyte.

Figure 8 shows the volumetric density of red cells relative to the leukocyte position. As for the velocity fields presented above, the average is computed on the condition that $d<0.4r_o$. The different relative stiffnesses lead to significantly different red cell distributions, though in all cases there is a high (nearly unity in cases) red cell density just upstream of the leukocyte. In Fig. 8(e), which shows the strongly marginating case for the relatively stiffest cells, we see a clear biconcave shaped cell leaning on the leukocyte. Its position must be very stable to yield these contours, and indeed in the randomly selected snapshots shown in Fig. 9(c), we typically see the corresponding cell. This configuration is less stable for less blunt mean flow profiles, but there is still commonly a red cell that appears to lean on the leukocyte. This can be seen in the red-cell density contours [Fig. 8(f)] and instantaneous visualizations [Fig. 9(d)], but its position relative to the leukocyte tends to vary and it comes off more frequently. Figures 8(a) and 8(b) show that the more flexible red cells also lean on the leukocyte's upstream side, but they tend to deform significantly, wrapping around the stiffer leukocyte. This can also be seen in the snapshots shown in Figs. 9(a) and 9(b). Even for the more weakly marginating case, a red cell is almost always leaning on the leukocyte; the density contours in Fig. 8(b) are near unity here. However, the leukocyte spends less time very near the wall in this case compared to that shown in Fig. 8(a). Intermediate red-cell stiffness cases [Figs. 8(c) and 8(d)] display a behavior that is, as expected, intermediate between these two extremes.

The picture that emerges from the observations of the leaning cells is that they somehow assist in holding the leukocyte on or near the wall, but the complexity of the viscous flow multibody dynamics of the mechanism make it difficult to diagnose in quantitative detail. Animations of the cells clearly show that when present the leaning cell slows the rotation of the leukocyte. It can be effective in this capacity because of the large area of small gap size between it and the leukocyte. It appears that the leaning cell is relatively stable in this location because it is the stagnation point in the frame of the leukocyte, as can be seen from the velocity field visualization in Fig. 7. The slowly rolling leukocyte tends to lift the leaning cell, but the viscous interaction with the moving wall tends to pull its bottom half leftward bringing it lower. A consequence of slowing the leukocyte's rotation is that it behaves more as a scrapper, pushing red cells approaching

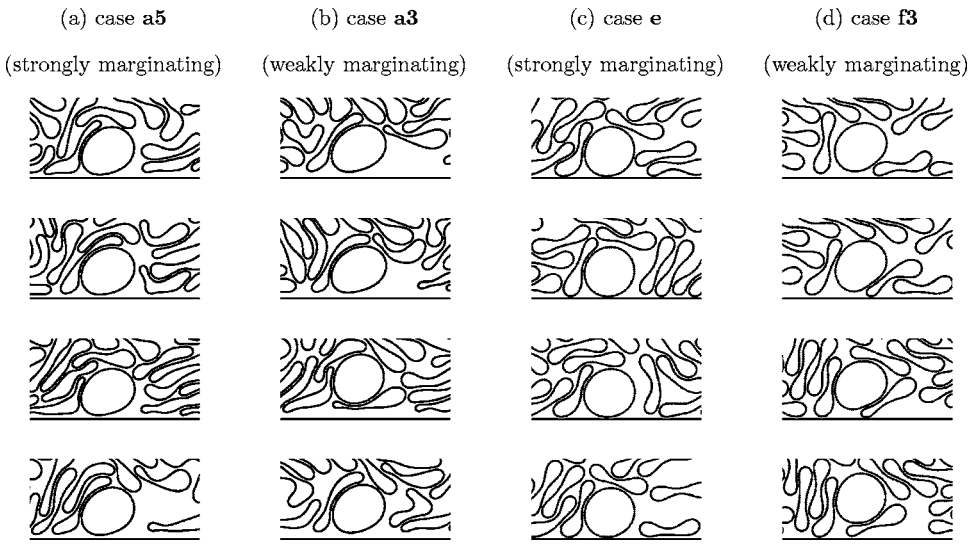

FIG. 9. Visualizations of leukocyte's neighborhood for strongly and weakly marginating cases for relatively flexible and stiff red cells.

from the right out the way and not allowing them to come under the leukocyte, lifting it off the wall. This is difficult to characterize for marginating or weakly marginating cases, since it is a rare event—the leukocyte infrequently leaves the wall. However, at higher flow rates, the leukocyte is almost immediately moved off the wall. For case **b**, red-cell density averaged on the condition that $d<0.4r_o$ clearly show a red cell coming under the leukocyte when it is close to the wall [Fig. 10(a)], as do instantaneous visualizations of the leukocyte's environment [Fig. 10(b)].

B. Fåhræus-Lindqvist effect and the mean leukocyte standoff distance

The Fåhræus-Lindqvist effect describes the observation that the apparent viscosity of blood flow in small tubes is lower than expected for Poiseuille flow. It is associated with a cell free layer that forms adjacent to the vessel (or tube) wall, which has been observed both in *in vitro*[40,41] and *in vivo*[38,42] experiments. The cell-free layer is typically less than a cell dimension thick. In absence of red cell aggregation, or at higher (typical physiological[42]) shear rates, the layer appears to thicken slowly with increasing flow rate.[40] Simulations with a single rigid two-dimensional red cell encountering a model wall-bound leukocyte suggest that the thickness of the cell-free layer might be important for adhesion dynamics.[17] On the whole, this cell-free layer seems inconsistent with the leukocyte being brought into contact with the vessel wall.

Our two-dimensional model also has a cell-free layer, which can be seen both in the visualizations of Fig. 2 and the hematocrit profiles shown in the bottom half of Fig. 11. At the slowest flow rate, the red cell density becomes finite just above $y=0.2r_o$, which was the maximum range of the repulsion (6). The thickness of this layer then increases with flow rate. The behavior of the leukocyte appears to be tied somehow to this layer: the most probable leukocyte distance from the wall, as seen in the top half of Fig. 11, corresponds to the point where the red-cell density profile begins to become significant. As was clear in Sec. III C, the distribution peak is higher at lower flow rates because the leukocyte spends considerably more time in the middle of the vessel at higher flow rates.

In Fig. 12, we examine this distance more closely by plotting the most probable leukocyte distance from the wall, which corresponds to the edge of the plasma-only wall layer, against the velocity of the leukocyte averaged on the condition that it is closer to the wall than its most probable position. We see that these quantities follow a scaling close to $d\sim\sqrt{U_\ell}$, which might be expected for a lubrication mechanism lifting an asymmetric object moving near to a wall, assuming motion away from the wall is resisted by an approximately constant force. Hydrodynamic mechanisms have

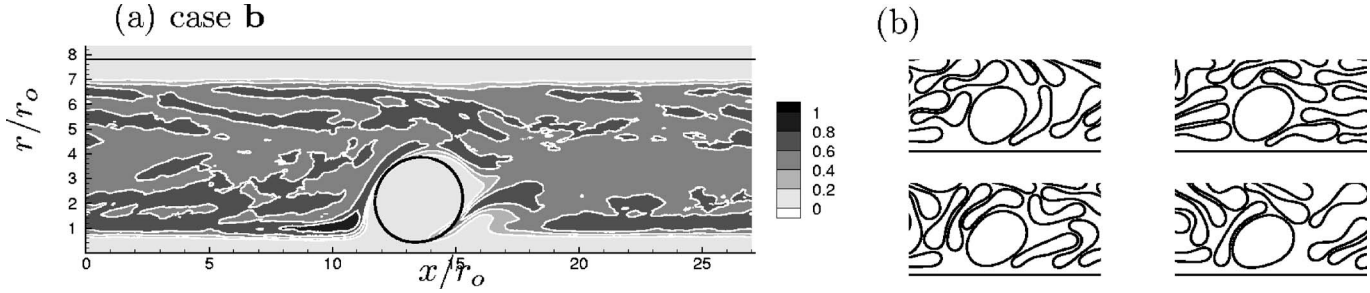

FIG. 10. (a) Red cell density for $d<0.4r_o$ case **b**; (b) randomly selected visualizations of the leukocytes neighborhood. The $d<0.4r_o$ statistical sample is smaller in this case than those in Fig. 8, which leads to choppier contours.

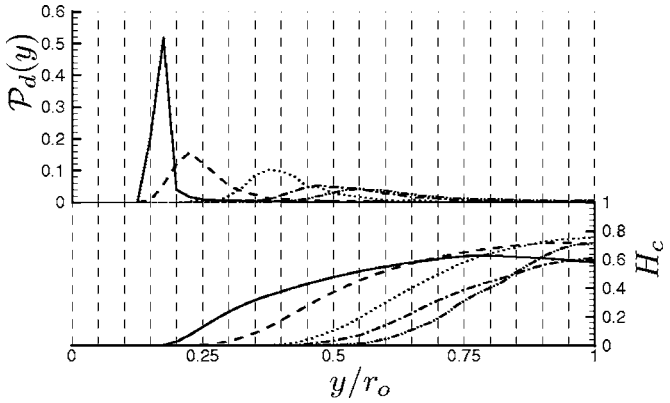

FIG. 11. (Top) Probability distribution of leukocyte wall distance; (bottom) red-cell density close to the wall. The lines show the *-cases in Table I: –·–· **a5**, –·– **b**, ··· **c**, - - -**d2**, and — **e**.

been suggested to be responsible in setting up the cell-free layers,[5] but it is unclear why it should be resisted by a constant force. In actuality, we might expect the exponent to be somewhat less than 1/2 as observed since the core should become harder to compress as the core-flow cell density increases, becoming incompressible in the limit of complete compaction of the cells.

This picture is supported by a numerical experiment flowing in a single red cell in a $13.5r_o \times 13.5r_o$ steamwise-periodic channel. The downward force was applied to points on the cell further from the wall than the cell's centroid y_c according to $f_y = -K(y - y_c)$, where the spring constant $K = 0.54T$ was selected to match one point on the $d \propto U^{0.43}$ curve in Fig. 12. The u^∞ was adjusted, and the resulting cell's wall distance is plotted against its velocity in Fig. 12. These points are well fitted by $d \propto U^{0.5}$. The tank-treading behavior that these cells undergo is similar to that observed in actual blood cells when the hematocrit is high enough.[43]

While we see that the thickness of the wall associated cell-free layer scales approximately as if upward motion were opposed by a constant (height independent) force, it is less clear why this should be the case. The return of the cell

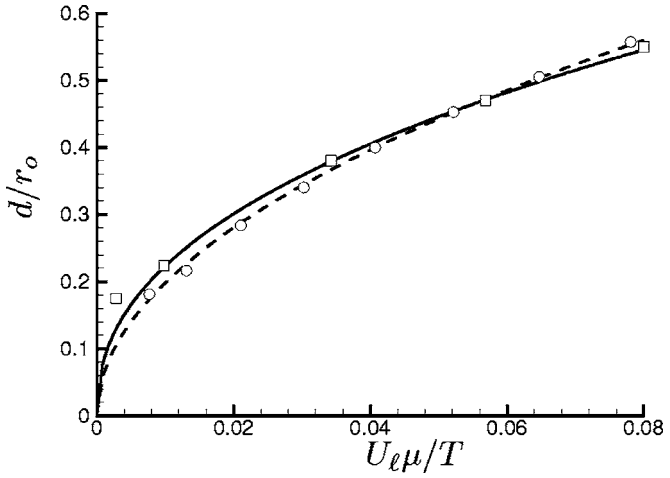

FIG. 12. Leukocyte wall distance versus its speed □ for the *-marked cases in Table I with fit — $d = 1.2U^{0.43}$. The ○ show the same for the single red cell test cases discussed in the text with fit - - - $d = 1.4U^{0.5}$.

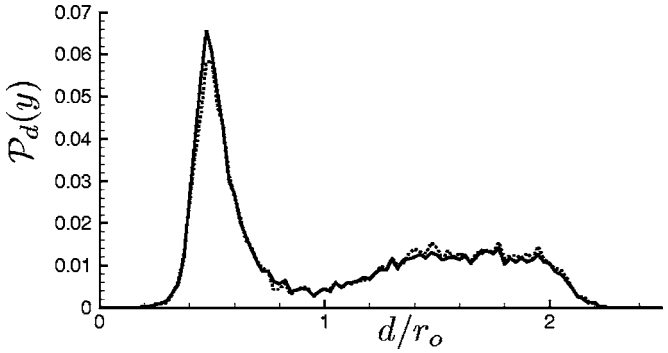

FIG. 13. Probability distribution of leukocyte distance from the wall for case **a2** —— and case **a2** with M_ℓ and T_ℓ tripled ···.

into the dense cell region requires displacement of cells and fluid. If we regard the cells as rigid and fixed in their relative positions, then they could be regarded as a porous medium. In this case, the resistance would be dominated by the smallest gap size the displaced fluid must negotiate. Our repulsion model restricts this to be close to $0.2r_o$. But a porous medium model does not of itself provide a mechanism for actively pushing of the red cells toward the wall, which presumably arises from their kinematic interactions. It seems that the mean wall distance position must involve a balance between a tendency for the cell-rich core to expand and the lubrication forces pushing cells away from the wall. Though the details of these factors remain unclear, the observed scaling suggests that the mechanism involves lubrication forces.

It is also still unclear why the most probable leukocyte distance from the wall corresponds so closely to the end of the cell-free layer. Because of its symmetry the leukocyte itself has no tendency to migrate away from the wall. Though our leukocyte can undergo small but finite deformations, tripling its stiffness has a negligible effect on its distribution in the channel, as is shown for case **a3** in Fig. 13. This suggests that it is the interactions of the leukocyte with its asymmetric red cell environment that provides a lubrication like lift. The geometry of the wall and the leaning red cell is somewhat reminiscent of the journal bearing, with the leaning cell forming the low pressure side and the wall the high pressure side. The apparent lubrication scaling of the data is consistent with this too, but the cell laden flow is clearly more complex. It seems to be lubrication trends along with the complex interactions of the cells and the hydrodynamic fields that leads to the similar height. This tie-in to the near wall dynamics is consistent with the results in Fig. 6, which shows that $r_o \sigma_w / u_m$ is a key parametric predictor of margination.

V. SUMMARY

Despite the approximations in the physical model, the simulations results show qualitative agreement with several experimental observations. In particular, we see decreased margination with increasing shear, blunting of velocity profiles at higher shear rates, and the existence of a cell-free layer adjacent the vessel wall that thickens with flow speed.

At low shear rates, the leukocytes marginate without red cell aggregation, which suggests that aggregation is unnecessary for margination.

Though a significant variation of the relaxation time scale relative to the advective time scale significantly changed the flow about the leukocyte when it was near the wall, it only slightly changed the marginating characteristics. The leukocyte was only slightly more prone to marginate with more flexible red cells. In these cases, the more flexible cells upstream of the leukocyte appeared more effective at slowing its rotation, making it more like a scraper and better able to deflect oncoming red cells, which might otherwise lift it off the wall. The relative insensitivity to red cell flexibility, suggests that it is their mismatched size or shape which is more important in promoting margination. Segregation experiments have shown that larger particles can accumulate in either higher or lower strain-rate regions (e.g., Krishnan *et al.*[44]). Further investigations into what geometric properties of the cells lead to the observed behavior are warranted.

It was observed in all cases that the most probable leukocyte position was on the edge of the near-wall cell-free layer, and that the thickness of this layer nearly followed a lubrication scaling assuming that motion away from the wall was resisted by a constant force. Tests with a single red cell subjected to an artificial constant force also showed a similar lubrication scaling, though the origin of this force in the many cell cases and why it should be approximately constant remain unclear. It was observed that the cell-free layer thickens at higher flow rates which seems to put the leukocyte into a less stable configuration with respect to the red cells. Visualizations suggest that the leaning red cell is more likely to be dislodged if it is positioned further from the wall. This mechanism potentially explains the observation that low molecular weight dextran inhibits margination and adhesion. Since viscosity increases with the addition of dextran, so will lubrication forces which in turn will increase red cell and leukocyte distance from the wall. For adhesion, the implications of the increasing standoff distance might be more direct since it could also inhibit the short ranged selectin-ligand binding that is necessary for capture. Proving the physiological relevance of the mechanisms we observed in our model system will require further study.

ACKNOWLEDGMENTS

The author is grateful for fruitful discussions with R. D. Moser early on in this effort and with H. Zhao who helped formalize the area preserving constraint.

[1] T. A. Springer, "Traffic signals on endothelium for lymphocyte circulation and leukocyte emigration," Annu. Rev. Fluid Mech. **57**, 827 (1995).
[2] K. B. Abbitt and G. B. Nash, "Rheological properties of the blood influencing selectin-mediated adhesion of flowing leukocytes," Am. J. Physiol. Heart Circ. Physiol. **285**, H229 (2003).
[3] G. W. Schmid-Schönbein, S. Usami, R. Skalak, and S. Chien, "The interaction of leukocytes and erythrocytes in capillary and postcapillary vessels," Microvasc. Res. **19**, 45 (1980).
[4] R. H. Phibbs, "Distribution of leukocytes in blood flowing through arteries," Am. J. Physiol. **210**, 919 (1966).
[5] T. W. Secomb, "Mechanics of red blood cells and blood flow in narrow tubes," in *Modeling and Simulation of Capsules and Biological Cells*, edited by C. Pozrikidis (Chapman & Hall/CRC, Boca Raton, 2003), pp. 163–196.
[6] R. J. Melder, J. Yuan, L. L. Munn, and R. K. Jain, "Erythrocytes enhance lymphocyte rolling and arrest *in vivo*," Microvasc. Res. **59**, 316 (2000).
[7] H. L. Goldsmith and S. Spain, "Margination of leukocytes in blood flow through small tubes," Microvasc. Res. **27**, 204 (1984).
[8] U. Nobis, A. R. Pries, G. R. Coklet, and P. Gaehtgens, "Radial distribution of white cells during blood flow in small tubes," Microvasc. Res. **29**, 295 (1985).
[9] K. B. Abbitt and G. B. Nash, "Characteristics of leukocyte adhesion directly observed in flowing whole blood *in vitro*," Br. J. Haematol. **112**, 55 (2001).
[10] J. C. Firrell and H. H. Lipowsky, "Leukocyte margination and deformation in mesenteric venules of rat," Am. J. Physiol. Heart Circ. Physiol. **256**, H1667 (1989).
[11] M. J. Pearson and H. H. Lipowsky, "Influence of erythrocyte aggregation on leukocyte margination in postcapillary venules of rat mesentery," Am. J. Physiol. Heart Circ. Physiol. **279**, H1460 (2000).
[12] M. J. Pearson and H. H. Lipowsky, "Effect of fibrinogen on leukocyte margination and adhesion in postcapillary venules," Microcirculation (Philadelphia) **44**, 295 (2004).
[13] A. S. Popel, P. C. Johnson, M. V. Kameneva, and M. A. Wild, "Capacity for red blood cell aggregation is higher in athletic mammalian species than in sedentary species," J. Appl. Physiol. **77**, 1790 (1994).
[14] C. Sun, C. Migliorini, and L. L. Munn, "Red blood cells initiate leukocyte rolling in postcapillary expansions: a lattice Boltzman analysis," Biophys. J. **85**, 208 (2003).
[15] C. Sun and L. L. Munn, "Particulate nature of blood determines macroscopic rheology: A 2-d lattice Boltzmann analysis," Biophys. J. **88**, 1635 (2005).
[16] M. R. King, D. Bansal, M. B. Kim, and I. H. Sarelius, "The effect of hematocrit and leukocyte adherence on flow direction in the microcirculation," Ann. Biomed. Eng. **32**, 803 (2004).
[17] C. Migliorini, Y. Qian, H. Chen, E. B. Brown, R. K. Jain, and L. L. Munn, "Red blood cells augment leukocyte rolling in a virtual blood vessel," Biophys. J. **83**, 1834 (2002).
[18] C. Pozrikidis, "Axisymmetric motion of a file of red blood cells through capillaries," Phys. Fluids **17**, 031503 (2005).
[19] C. Pozrikidis, "Numerical simulation of the flow-induced deformation of red blood cells," Ann. Biomed. Eng. **31**, 1194 (2003).
[20] G. Breyiannis and C. Pozrikidis, "Simple shear flow of suspensions of elastic capsules," Theor. Comput. Fluid Dyn. **13**, 327 (2000).
[21] G. Kanzow, A. R. Pries, and P. Gaehtgens, "Analysis of the hematocrit distribution in the mesenteric micro-circulation," Int. J. Microcirc.: Clin. Exp. **1**, 67 (1982).
[22] S. D. House and H. H. Lipowsky, "Microvascular hematocrit and red cell flux in rat cremaster muscle," Am. J. Physiol. Heart Circ. Physiol. **252**, H211 (1987).
[23] J. Q. Lu, P. Yang, and X.-H. Hu, "Simulations of light scattering from a biconcave red blood cell using the finite-difference time-domain method," J. Biomed. Opt. **10**, 024022 (2005).
[24] G. P. Downey, D. E. Doherty, B. Schwab III, E. L. Elson, P. M. Henson, and G. S. Worthen, "Retention of leukocytes in capillaries: role of cell size and deformability," J. Appl. Physiol. **69**, 1767 (1990).
[25] R. L. Whitmore, *Rheology of the Circulation* (Pergamon, Oxford, 1968).
[26] K.-M. Jan and S. Chien, "Role of surface electric charge in red blood cell interactions," J. Gen. Physiol. **61**, 638 (1973).
[27] Y. Suzuki, N. Tateishi, and N. Maeda, "Electrostatic repulsion among erythrocytes in tube flow, demonstrated by the thickness of the marginal cell-free layer," Biorheology **35**, 155 (1998).
[28] C. Pozrikidis, *Boundary Integral and Singularity Methods for Linearized Viscous Flow* (Cambridge University Press, Cambridge, 1992).
[29] C. Canuto, M. Y. Hussaini, A. Quarteroni, and T. A. Zang, *Spectral Methods in Fluid Dynamics* (Springer-Verlag, Berlin, 1987).
[30] H. Hashimoto, "On the periodic fundamental solutions of the Stokes equations and their application to viscous flow past a cubic array of cylinders," J. Fluid Mech. **5**, 317 (1959).
[31] D. Frenkel and B. Smit, *Understanding Molecular Simulation* (Academic Press, San Diego) (1996).
[32] R. W. Hockney and J. W. Eastood, *Computer Simulation Using Particles* (Institute of Physics, Bristol, 1988).

[33]U. Essemann, L. Perera, M. L. Berkowitz, T. Darden, H. Lee, and L. G. Pedersen, "A smooth particle mesh Ewald method," J. Chem. Phys. **103**, 8577 (1995).
[34]D. Saintillan, E. Darve, and E. S. G. Shaqfeh, "A smooth particle-mesh Ewald algorithm for Stokes suspension simulations: The sedimentation of fibers," Phys. Fluids **17**, 033301 (2005).
[35]E. Metsi, "Large scale simulations of bidisperse emulsions and foams," Ph.D. thesis, University of Illinois at Urbana-Champaign (2000).
[36]M. E. Staben, A. Z. Zinchenko, and R. H. Davis, "Motion of a particle between two parallel plane walls in low-Reynolds-number Poiseuille flow," Phys. Fluids **15**, 1711 (2003).
[37]A. S. Popel and P. C. Johnson, "Microcirculation and hemorheology," Annu. Rev. Fluid Mech. **37**, 43 (2005).
[38]D. S. Long, "Microviscometric analysis of microvascular hemodynamics *in vivo*," Ph.D. thesis, University of Illinois at Urbana-Champaign, Urbana, Illinois (2004).
[39]R. J. Melder, L. L. Munn, S. Yamada, C. Ohkubo, and R. K. Jain, "Selective- and integrin-mediated T-lymphocyte rolling and arrest on TNF-α-activated endothelium: augmentation by erythrocytes," Biophys. J. **69**, 2131 (1995).
[40]W. Reinke, P. Gaehtgens, and P. C. Johnson, "Blood viscosity in small tubes: effect of shear rate, aggregation and sedimentation," Am. J. Physiol. Heart Circ. Physiol. **253**, H540 (1987).
[41]C. Alonso, A. R. Pries, O. Kiesslich, D. Lerche, and P. Gaehtgens, "Transient rheological behavior of blood in low-shear tube flow: velocity profiles and effective viscosity," Am. J. Physiol. Heart Circ. Physiol. **268**, H25 (1995).
[42]H. H. Lipowsky, S. Usami, and S. Chien, "*In vivo* measurements of 'apparent viscosity' and microvessel hematocrit in the mesentry of the cat," Microvasc. Res. **19**, 297 (1980).
[43]T. M. Fisher, "A comparison of the flow behavior of disc shaped versus elliptic red blood cells (RBC)," Blood Cells **4**, 453 (1978).
[44]G. P. Krishnan, S. Beimfohr, and D. T. Leighton, "Shear-induced radial segregation in bidisperse suspensions," J. Fluid Mech. **321**, 371 (1996).